Available online at www.sciencedirect.com

ScienceDirect

Procedia CIRP 75 (2018) 75–80

www.elsevier.com/locate/procedia

15th CIRP Conference on Computer Aided Tolerancing – CIRP CAT 2018

Shape Transformation Perspective for Geometric Deviation Modeling in Additive Manufacturing

Zuowei Zhu[a]*, Nabil Anwer[a], Luc Mathieu[a]

[a] *LURPA, ENS Paris-Saclay, Univ. Paris-Sud, Université Paris-Saclay, 94235 Cachan, France*

* Corresponding author. Tel.: +33-(0)147402765; fax: +33-(0)147402220. *E-mail address:* zzhu@ens-paris-saclay.fr

Abstract

Geometric deviations arising from multiple variation sources in Additive Manufacturing (AM) process chain have been a major issue regarding product quality. Therefore, effective modeling of the geometric deviations is becoming critical for AM. In this paper, in-plane geometric deviations are investigated based on the assumption that typical deviation sources in AM can be mapped to different transformations (scaling, rotation, translation) on the nominal shape. By defining transformation parameters, analytical deviation models of regular shapes can be derived in the deviation space, and calibrated based on measurement data. A case study is presented to show the effectiveness of the proposed approach.

Keywords: Additive Manufacturing, Deviation Modeling, Shape Transformation

1. Introduction

As a manufacturing technology that builds three-dimensional products by successively adding material layer by layer under computer control, Additive Manufacturing (AM) distinguishes from traditional manufacturing technologies for its ability to manufacture products with complex shapes, intricate internal structures and multiple materials. Therefore, AM has gained extensive research attention and continuous development in recent years.

Geometric deviations remain a major issue that hinders the further development of AM. These geometric deviations are induced by multiple sources underlying in different workflows of the AM process. In the digital workflow where the input data are prepared for the machine, chordal deviations are introduced during the translation from CAD model to the approximated STL facet model. In the physical workflow that transforms raw materials into end product [1], machine errors, material shrinkage and distortion as well as the staircase effect bring about different patterns of deviations. Support removal during post-processing of the product also affects the surface quality of the final product. Based on [2], Fig.1 provides a cause-and-effect diagram of geometric deviations in AM.

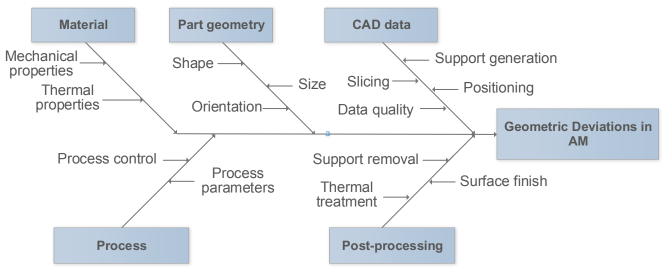

Fig. 1. Cause-and-effect diagram of geometric deviations in AM.

Considerable research efforts have been devoted to the effective modeling of geometric deviations in each stage of the AM process and the derivation of compensation plans to control deviations. To decrease the approximation deviation introduced in translation from CAD model to STL file, STL modification algorithms [3,4] are proposed to locally modify the STL facets based on criteria like chordal error, cusp height and form error. Adaptive slicing approaches are proposed to minimize the deviation induced by the staircase effect [5,6]. New file formats, such as Steiner patch [7] and Additive Manufacturing Format (AMF) [8], are proposed that use curved surface patches and result in a more accurate approximation of the CAD surface.

2212-8271 © 2018 The Authors. Published by Elsevier B.V.
Peer-review under responsibility of the Scientific Committee of the 15th CIRP Conference on Computer Aided Tolerancing - CIRP CAT 2018.
10.1016/j.procir.2018.04.038

Another major branch of research is focused on the machine-related and process-related deviation modeling and compensation based on simulation or measurement data. The effect of Fused Deposition Modeling (FDM) and Stereolithography (SLA) machine errors on deviations are studied in [9] and [10]. Thermal behavior and influence of process parameters on thermal shrinkage of powder-bed AM processes are investigated by [11] and [12]. To address the effective modeling of shrinkage deviation, Huang et al. intuitively propose the classification of in-plane [13] and out-of-plane [14] deviations, denoting the shrinkage inside each two-dimensional (2D) slice and along the build direction respectively. The focus of these in-plane deviation modeling methods has been the parametric modeling of the deviation profile. By observing the distribution of deviation, a basis function is prescribed and calibrated according to new observations and new shapes.

Researchers from the tolerancing domain are also paying attention to AM. An enriched voxel-based volumetric representation is proposed by Moroni et al. [15] that overcomes the limitations of current tolerancing standards in the application of AM. A process-oriented deviation model has been proposed by Dantan et al. [16] to represent the overall deviation by a combination of deviation modes, with each mode corresponding to a deviation pattern caused by a specific source. Our previous works [17, 18] envision the application of Skin Model Shapes (SMS) [19] in AM, as well as proposing a Fourier-Series expansion (FSE) based method for in-plane deviation modeling and a shape transformation method for SMS generation. The idea of the FSE method is to represent the actual 2D product shape with a function of its polar radius with respect to its polar angle in the polar coordinate system (PCS). The function is approximated with a truncated FSE and the in-plane deviation is evaluated as the difference between the function value and the nominal radius at each angle. However, in order to achieve a satisfactory accuracy, a high-order expansion is needed, yielding a large number of parameters and the number increases with the shape complexity. Therefore, in this paper, we propose a new transformation perspective to capture the in-plane systematic deviation patterns by investigating variations of the nominal shape during the AM process, thus significantly reducing the number of parameters.

2. The shape transformation perspective for in-plane deviation modeling

The layer-wise characteristic of AM has motivated research on the modeling of in-plane deviation. In order to facilitate the representation of in-plane deviation, the PCS has been adopted in many existing approaches to represent the deviation as the difference between the radii of the actual shape $r(\theta)$ and the nominal shape $r_0(\theta)$ at different locations $\theta \in [0,2\pi]$ around the 2D shape boundary. The actual shape denotes the shape of a layer of the fabricated product that can be reconstructed from the measurement data, as will be explained in detail in Section 3.2.The nominal shape is the input shape of the corresponding layer that can be extracted from the CAD model, as illustrated in Fig.2. Thus, the deviation is represented as Eq.1.

$$\Delta r(\theta) = r(\theta) - r_0(\theta) \tag{1}$$

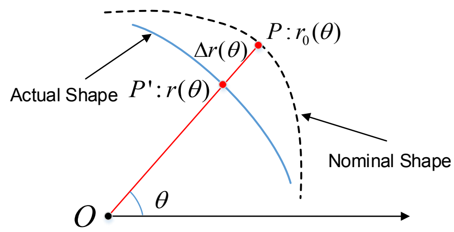

Fig. 2. In-plane deviation represented in PCS.

Here we propose the definition of the deviation space – a 2D space established based on PCS and denoted as $(\theta, \Delta r)$. The deviation patterns can be investigated in the deviation space by studying the distribution of deviation Δr with respect to θ. Intricate deviation sources underlying in the AM process result in the variations of the nominal shape. Take the FDM process as an example, the extruder positioning error may cause the displacement of the final shape in either X- or Y-direction of the machine coordinate system and the heating and cooling process leads to thermal shrinkage and material distortion. Therefore, it is reasonable to make an assumption that such variations can be mapped to transformations of the nominal shape, in which three transformation effects can be defined by a set of parameters: the translation in X- and Y- direction $\Delta x, \Delta y$ to consider the extruder positioning error, the scaling Sx, Sy along X- and Y-direction to consider the shrinkage effect and the rotation φ with respect to the origin to account for the unexpected rotation due to machine axis and setup errors.

3. In-plane deviation model formulation and estimation

3.1. Model Formulation

Based on these parameters, the transformation of the nominal shape in the Cartesian Coordinate System (CCS) can be defined with homogeneous transformation matrices. As shown in Eq.2, M_S, M_R, M_T represent transformation matrices of scaling, rotation and translation respectively.

$$M_S = \begin{bmatrix} s_x & 0 & 0 \\ 0 & s_y & 0 \\ 0 & 0 & 1 \end{bmatrix} M_R = \begin{bmatrix} 1 & 0 & \Delta x \\ 0 & 1 & \Delta y \\ 0 & 0 & 1 \end{bmatrix} M_T = \begin{bmatrix} \cos(\varphi) & -\sin(\varphi) & 0 \\ \sin(\varphi) & \cos(\varphi) & 0 \\ 0 & 0 & 1 \end{bmatrix} \tag{2}$$

Suppose that the coordinate of a point on the nominal shape is (x, y), multiplying the original coordinate vector with transformation matrices yields a new vector containing the transformed coordinates (x_T, y_T).

$$(x_T, y_T, 1)^T = M_S M_R M_T (x, y, 1)^T \tag{3}$$

Solving (x, y) with respect to (x_T, y_T) based on Eq.2 and Eq.3, we get

$$\begin{aligned} x &= \left[(y_T - \Delta y)\cos(\varphi) - (x_T - \Delta x)\sin(\varphi)\right] / s_y \\ y &= \left[(y_T - \Delta y)\sin(\varphi) + (x_T - \Delta x)\cos(\varphi)\right] / s_x \end{aligned} \tag{4}$$

Based on Eq.4, we will discuss the shape deviation representation in PCS for two kinds of shapes: the circular shape and the polygonal shape, among which the latter can be easily extended to represent deviations for other polygonal shapes.

For a circular shape, its polar representation is

$$r(\theta) = r_0, \theta \in [0, 2\pi] \tag{5}$$

This representation is derived by substituting the Cartesian coordinates with $x = r\cos(\theta), y = r\sin(\theta)$ in Eq.6.

$$x^2 + y^2 = r_0^2 \tag{6}$$

In order to calculate the deviations between the nominal shape and the transformed shape in PCS, their coordinates need to be calculated with respect to the same origin. Therefore, by substituting (x_T, y_T) with $x_T = r_T\cos(\theta), y_T = r_T\sin(\theta)$ in Eq.4 and combining Eq.4 with Eq.6, we get Eq.7, in which $\Theta = (s_x, s_y, \varphi, \Delta x, \Delta y)$ is the transformation parameter set.

$$\begin{aligned} & x(r_T, \theta, \Theta)^2 + y(r_T, \theta, \Theta)^2 = r_0^2 \\ & x(r_T, \theta, \Theta) = \left[(r_T\cos(\theta) - \Delta y)\cos(\varphi) - (r_T\sin(\theta) - \Delta x)\sin(\varphi) \right] / s_y \\ & y(r_T, \theta, \Theta) = \left[(r_T\cos(\theta) - \Delta y)\sin(\varphi) + (r_T\sin(\theta) - \Delta x)\cos(\varphi) \right] / s_x \end{aligned} \tag{7}$$

Resolving r_T with respect to θ, we can get the analytical polar representation of the transformed shape $r_T(\theta;\Theta)$, which is a quite long equation and cannot be properly presented in this paper, so the details of this equation will be omitted. Therefore, the shape deviation can be represented in the deviation space as Eq.8, in which $\varepsilon(\theta)$ is a random term to account for the aleatory variation in the shape profile and is assumed to have a normal distribution with mean 0 at each angle θ.

$$f(\theta;\Theta) = r_T(\theta;\Theta) - r_0 + \varepsilon(\theta) \tag{8}$$

With this function, we can make different tests of the shape deviations under various transformations by setting the values of transformation parameters Θ. Fig.3 illustrates 3 deviation patterns resulted from different transformation effects on a circular shape with $r_0 = 10$. The parameter values are set as $s_x = 0.98$ (Fig.3(a)), $\Delta x = 0.2$ (Fig.3(b)) and $s_x = 0.98, \varphi = \pi/9$ (Fig.3(c)). The shapes before and after transformation are shown on the right to illustrate the differences. Random term in Eq.8 is not considered here to emphasize the main patterns.

The study on deviation of polygonal shapes can be generalized to any convex shapes that can be approximated by a complex polygon through subdivision. A critical part in representing the shape deviations under transformations of a polygonal shape is to derive its polar representation. Unlike the circular shape that has uniform radius, the radius of the polygonal shape varies and has to be treated respectively for each edge. First of all, the vertices of a polygonal shape are ordered counter-clockwise, and the shape can be defined by a set of neighboring vertex pairs. For example, a polygonal shape with N vertices is defined as $\{[P_1, P_2], [P_2, P_3], ..., [P_{N-1}, P_N], [P_N, P_1]\}$, each vertex pair defines an edge of the shape. The polar coordinates of the end points of an edge are obtained through polar transformation, thus we get the angle range that the edge covers in the polar space. The problem now becomes how to derive the polar radius $r_0(\theta)$ of the shape at an arbitrary polar angle θ, which is the distance between the origin and the intersection point of one edge of the shape and a ray starting from the origin and pointing in the direction of θ. Since the angle range of each edge is known, it is easy to determine the edge that intersects with the ray of θ by finding the range that θ lies in. Suppose the intersected edge is $[P_m(x_m, y_m), P_n(x_n, y_n)]$ covering the angle range $[\theta_m, \theta_n]; m, n = 1, 2, ...N$, the radius at θ can be calculated following Eq.9.

$$\begin{aligned} & x(\theta) = x_m - t(\theta)(x_m - x_n), y(\theta) = y_m - t(\theta)(y_m - y_n) \\ & t(\theta) = \frac{y_m - \tan(\theta)x_m}{\tan(\theta)(x_n - x_m) + y_m - y_n}, \quad \theta \in [\theta_m, \theta_n] \\ & r_0(\theta) = \sqrt{x(\theta)^2 + y(\theta)^2} \end{aligned} \tag{9}$$

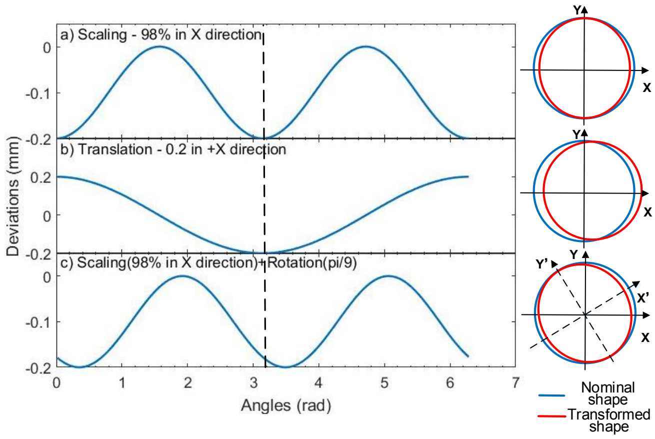

Fig. 3. Deviation of circular shape under (a) Scaling effect; (b) Translation effect; (c) Combined scaling and rotation effect.

The polar representation of the transformed shape can be derived in a similar manner, the difference lies in that the angle range of each edge should be changed due to the transformation effects. As can be seen in Fig.4, the radius of the transformed shape $r_T(\theta;\Theta)$ at θ is calculated based on the new positions of the vertices $P_m^{'}, P_n^{'}$, and the new positions are calculated following Eq.3 based on these transformation parameters Θ. Therefore, as shown in Eq.10, the shape deviation for a polygonal shape is parameterized as a discrete function of the nominal Cartesian coordinates of its vertices $(\boldsymbol{x}_0, \boldsymbol{y}_0)$ as well as transformation parameters Θ.

$$f(\theta;\Theta, \boldsymbol{x}_0, \boldsymbol{y}_0) = r_T(\theta;\Theta, \boldsymbol{x}_0, \boldsymbol{y}_0) - r_0(\theta;\boldsymbol{x}_0, \boldsymbol{y}_0) + \varepsilon(\theta) \tag{10}$$

Fig.5 illustrates 3 deviation patterns resulting from different transformation effects on a regular hexagon shape with circumscribed radius of 20mm. The parameter values are respectively set as $s_x = 0.98$ (Fig.5(a)), $\Delta x = 0.2$ (Fig.5(b)) and $s_x = 0.98, \varphi = \pi/60$ (Fig.5(c)). The shapes before and after transformation are shown on the right to illustrate the differences. Random term in Eq.10 is not considered here to emphasize the main patterns.

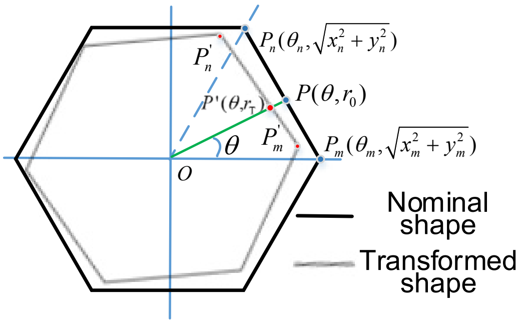

Fig. 4. Illustration of polygonal shape deviation under transformations.

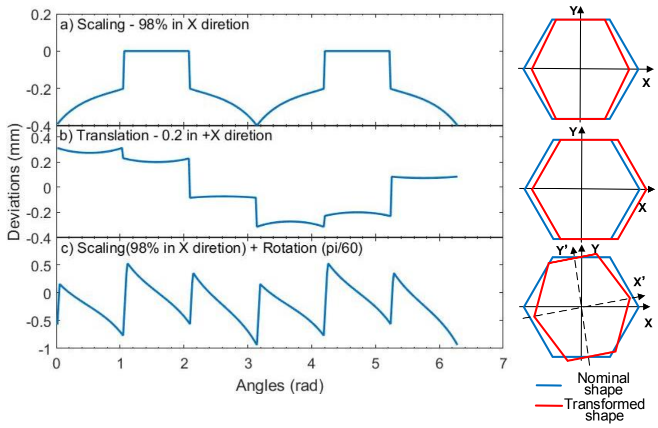

Fig. 5. Deviation of hexagon shape under (a) Scaling effect; (b) Translation effect; (c) Combined scaling and rotation effect.

3.2. Model estimation

In order to apply the parametric deviation model to fit the observed deviations, an effective estimation of the model parameters is essential. In this paper, the estimation will be conducted based on analysis of measurement data obtained from manufactured instances of a given product. The measurement data are given as point clouds that are densely collected on the product surface using a Coordinate Measuring Machine (CMM). Fig.6 provides a flowchart of the overall model estimation process.

To begin with, the 2D shape of a specific slice has to be reconstructed from the slice boundary points, which can be extracted from the point cloud according to the slice height calculated based on the input slice thickness. The extraction is done according to the following Eq.11.

$$\begin{aligned}&\forall P_m(x_m, y_m, z_m) \in \boldsymbol{P},\\&(x_m, y_m) \in \boldsymbol{S}^i, if\,(h_i - \lambda \le z_m \le h_i + \lambda),\\&i = 1,\dots,N_s; m = 1,\dots,M\end{aligned} \quad (11)$$

In Eq.11, P_m is a point among the all M points in the cloud $\boldsymbol{P}$, $\boldsymbol{S}^i$ is a collection of 2D points that belong to the ith slice among all N_s slices with slice height h_i, and λ is a threshold value that controls the density of the collected points in a slice, which is small compared to the layer thickness. Since the extracted points are densely distributed on the 2D slice boundary, by sequentially connecting the points with straight lines in the counter-clockwise direction, the actual 2D shape can be approximately reconstructed. Then both the CAD input shape and the actual shape are transformed into PCS to obtain $(\theta, r(\theta))$ and $(\theta, r_0(\theta))$. The origin of the PCS is chosen to be the same as the origin of the machine coordinate system. Thus the measured deviations are obtained following Eq.1.

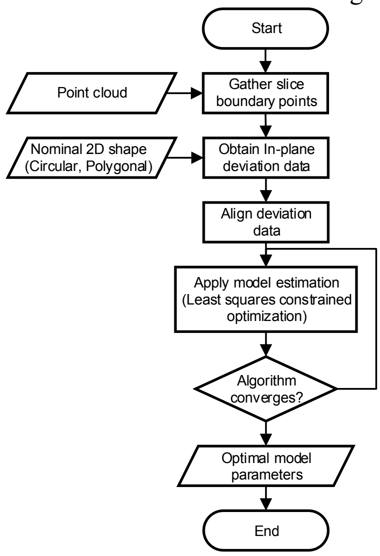

Fig. 6. Flowchart of the model estimation process.

An issue arises here that the measured points are not always uniformly distributed along the boundary, which results in the varied densities of points between layers and adds difficulty to calculation and comparison of deviations. We tackle this problem through an alignment process in which we evaluate the deviations at K angles that are uniformly distributed between 0 and 2π and denoted as $(\theta_1^{\mathrm{u}},\dots,\theta_K^{\mathrm{u}})$. Suppose that there are $L(L>K)$ measured deviations represented in the deviation space as $(\theta_1^{\mathrm{v}}, \Delta r(\theta_1^{\mathrm{v}})),\dots,(\theta_L^{\mathrm{v}}, \Delta r(\theta_L^{\mathrm{v}}))$, for a sample angle θ_i^{u}, two nearest neighboring angles $\theta_j^{\mathrm{v}}, \theta_{j+1}^{\mathrm{v}}$ and their corresponding deviations $\Delta r(\theta_j^{\mathrm{v}}), \Delta r(\theta_{j+1}^{\mathrm{v}})$ can be identified, then the deviation at this sample point can be calculated following Eq.12. The high-density of measured points ensures the accuracy of deviations calculated at these uniformly distributed points.

$$\Delta r(\theta_i^{\mathrm{u}}) = \frac{\Delta r(\theta_{j+1}^{\mathrm{v}}) - \Delta r(\theta_j^{\mathrm{v}})}{\theta_{j+1}^{\mathrm{v}} - \theta_j^{\mathrm{v}}}(\theta_i^{\mathrm{u}} - \theta_j^{\mathrm{v}}); \theta_i^{\mathrm{u}} \in (\theta_j^{\mathrm{v}}, \theta_{j+1}^{\mathrm{v}}], j = 1,\dots,L-1 \quad (12)$$

Our objective is to estimate the transformation parameters $\hat{\Theta}(\hat{s}_x, \hat{s}_y, \hat{\varphi}, \Delta\hat{x}, \Delta\hat{y})$ of Eq.8 that best fits the measured deviations $\Delta r(\theta^{\mathrm{u}})$. We propose to use a constrained optimization method based on a least-squares criterion that minimizes the squared difference between the model response $f(\theta^{\mathrm{u}})$ and measured deviation $\Delta r(\theta^{\mathrm{u}})$. The rationale of this method is shown as

$$\hat{\Theta} = \underset{s_x, s_y, \varphi, \Delta x, \Delta y}{\arg\min} \sum_{i=1}^{K}\left[f(\theta_i^{\mathrm{u}}; \Theta) - \Delta r(\theta_i^{\mathrm{u}})\right]^2 s.t.\begin{cases} s_x, s_y \in [1\text{-}\delta_s, 1+\delta_s] \\ \varphi \in [\text{-}\delta_r, \delta_r] \\ \Delta x, \Delta y \in [\text{-}\delta_t, \delta_t] \end{cases} \quad (13)$$

, in which $\delta_s, \delta_r, \delta_t$ are used to define constraint on the scaling, rotation and translation parameters respectively. Since the deviations are small compared to the product size, it is reasonable to limit them within a small range to facilitate the optimization process.

Different optimization methods can be adopted, among which we chose the built-in function *fmincon* of MATLAB to implement the proposed method. Starting from an initial point of the parameters $\Theta_0 = (1,1,0,0,0)$, the algorithm iteratively searches within the specified constraints of each parameter with trial steps to decrease the value of the objective function shown in Eq.(13). The convergence is met when the size of current step is less than a predefined step size tolerance and constraints are satisfied to within the predefined constraint tolerance.

3.3. Model Application

The proposed deviation model can be applied in tolerancing to generate SMS that are sample product shapes incorporating the geometric deviations. SMS are typically represented with discrete geometries, such as triangular meshes. In order to account for the 2D in-plane deviations in 3D SMS, we propose to apply the proposed deviation model in each slice to obtain deviated 2D shapes and then use a layer-connection method to connect pairs of neighboring slices to result in the 3D mesh model. Fig.7 illustrates the layer-connection method. The details of this method can be found in [18], and will not be discussed at length in this paper.

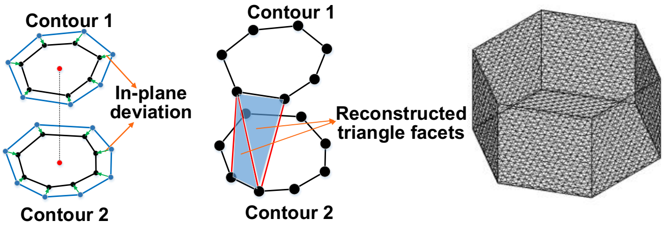

Fig. 7. The layer-connection method.

4. Case study

To validate the proposed method, we conduct the case study by printing a polygonal shape and modeling with the measured deviations. The example shape is a regular hexagon with circumscribed radius 20 and height 5. A comparison between the proposed method and the FSE method will be made regarding the model complexity and accuracy.

The Prusa i3 MK2 FDM printer is used to manufacture the part. The slice height is chosen as 0.2mm and the zigzag infill strategy is adopted. The part is measured by a 3D laser scanner Kreon Aquilon 50 mounted on a CMM. According to the calibration results, the measurement accuracy of the laser sensor is 0.002mm, which can be ignored compared to the geometric deviations. A total number of 795935 points are captured on the product surface, from which points of each slice are collected every 0.2mm with the threshold value λ (Eq.11) as 0.003 and converted into PCS. The deviations are evaluated at 360 uniformly distributed points on the slice boundary based on Eq.12. As an example, the deviation modeling result at the 6th slice is illustrated in Fig.8. Both the proposed method and the FSE method are used to model the observed deviations. For the latter, we chose different orders of expansion to test the modeling accuracy. The results given by 5th, 15th and 35th order expansion can be visualized in Fig.8 as compared to the proposed method. From the comparison, we can see that the proposed method prevails due to its ability to capture the sharp transitions at the corners of shape boundary with a far smaller number of parameters. While the FSE method tends to approximate the sharp transitions by overlapping multiple high-frequency components, so even the 35th order expansion fails to give a satisfactory approximation.

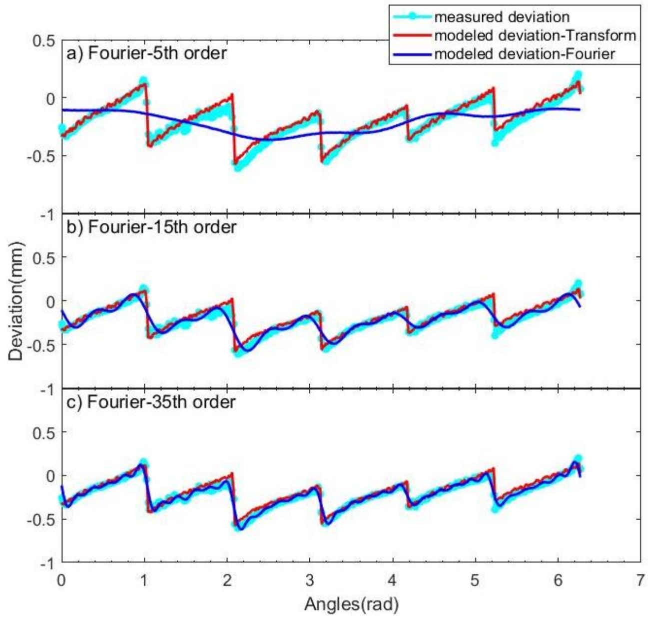

Fig. 8. Comparison between the modeling results yielded by the proposed method and FSE method of (a) 5th order; (b) 15th order; (c)35th order.

The modeling accuracy of the two methods is evaluated using the notation of Root Mean Square Error (RMSE) that measures the average deviation between the modeled deviation and the measured deviation. The RMSE of the proposed method and the 5th, 15th and 35th order FSE method as evaluated at each slice are calculated and shown in Fig.9, from which we can see that the proposed method reaches an accuracy that is comparable to the FSE method with more than 15 components, which contains a total number of 31 parameters. The significant reduction of parameters decreases the model complexity and improves model generalization.

Using both deviation models, the deviated 2D shape is calculated for each slice, and the layer-connection method is used to connect pairs of neighboring slices, yielding a 3D triangular mesh model as shown in Fig.10. The amplitude of deviations are highlighted with a color map on the surface. The proposed method better captures the sharp changes of deviations at corners of the shape, as observed in the measurement data, which proves the effectiveness of the method.

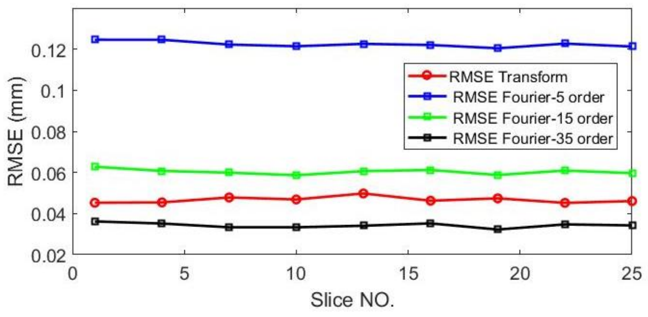

Fig. 9. Comparison of RMSE of both methods for each slice.

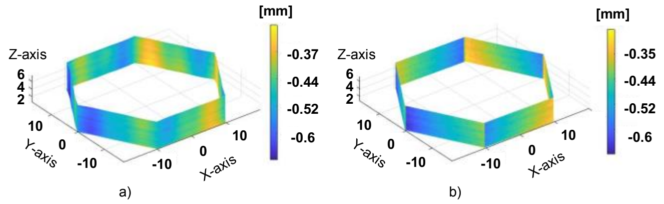

Fig. 10. SMS generated by (a) 35th order FSE method; (b) proposed method.

5. Conclusion and outlook

Modeling of geometric deviations is an important concern for AM. In this paper, in-plane geometric deviations are investigated based on a transformation perspective that maps effects of AM deviation sources to different transformation effects on the nominal shape. Parametric deviation models are formulated for circular and polygonal shapes based on the transformation parameters. This transformation perspective implies the consideration of deviation sources in AM and is based on the geometric information of the designed shape, therefore, compared to the FSE method that approximates the actual shape using high-order Fourier Series, the model generalizes well to different shapes and the model complexity is significantly reduced. Nevertheless, limitations of the method also exist. The transformation parameters are currently treated as constants and applied to the overall shape, thus the model doesn't generalize well for deviations resulted from location-dependent deviation sources. The current model estimation procedure is lacking in a learning capability, so existing parameter settings cannot be effectively reused as knowledge to facilitate the generalization to new process conditions.

Apart from overcoming these limitations, the future work will also be focused on improving the model based on geometric deviation data obtained from AM process simulations. Extension of the method to more complex freeform shapes will be studied and further applications of the method on SMS will be exploited. The derivation of geometric compensation on the designed geometry based on the proposed model is also worth investigating.

Acknowledgements

This research has benefitted from the financial support of China Scholarship Council (first author).

References

[1] Thompson K, Moroni G, Vaneker T, et al. Design for Additive Manufacturing: Trends, Opportunities considerations, and constraints. CIRP Annals-Manufacturing Technology 2016; 65 (2):737-760.
[2] Rehme O. Cellular design for laser freeform fabrication. Göttingen: Cuvillier; 2010.
[3] Navangul G, Paul R, Anand S. Error minimization in layered manufacturing parts by stereolithography file modification using a vertex translation algorithm. Journal of Manufacturing Science and Engineering 2013; 135(3): 031006.
[4] Zha W, Anand S. Geometric approaches to input file modification for part quality improvement in additive manufacturing. Journal of Manufacturing Processes 2015; 20:465-477.
[5] Siraskar N, Paul R, Anand S. Adaptive Slicing in Additive Manufacturing Process Using a Modified Boundary Octree Data Structure. Journal of Manufacturing Science and Engineering 2015; 137(1):011007.
[6] Panhalkar N, Paul R, Anand S. Increasing Part Accuracy in Additive Manufacturing Processes Using a kd Tree Based Clustered Adaptive Layering. Journal of Manufacturing Science and Engineering 2014; 136(6): 061017.
[7] Paul R, Anand S. A new Steiner patch based file format for additive manufacturing processes. Computer-Aided Design 2015; 63:86-100.
[8] ISO / ASTM52915-16, Standard Specification for Additive Manufacturing File Format (AMF) Version 1.2, ASTM International, West Conshohocken, PA, 2016, www.astm.org.
[9] Tong K, Amine Lehtihet E, Joshi S. Parametric error modeling and software error compensation for rapid prototyping. Rapid Prototyping Journal 2003; 9(5):301-313.
[10] Tong K, Joshi S, Amine Lehtihet E. Error compensation for fused deposition modeling (FDM) machine by correcting slice files. Rapid Prototyping Journal 2008; 14(1):4-14.
[11] Foteinopoulos P, Papacharalampopoulos A, Stavropoulos P. On thermal modeling of Additive Manufacturing processes. CIRP Journal of Manufacturing Science and Technology 2018; 20:66-83.
[12] Raghunath N, Pandey PM. Improving accuracy through shrinkage modelling by using Taguchi method in selective laser sintering. International journal of machine tools and manufacture 2007; 47(6):985-995.
[13] Wang A, Song S, Huang Q, Tsung F. In-plane shape-deviation modeling and compensation for fused deposition modeling processes. IEEE Transactions on Automation Science and Engineering 2017; 14(2):968-976.
[14] Jin Y, Qin SJ, Huang Q. Offline predictive control of out-of-plane shape deformation for additive manufacturing. Journal of Manufacturing Science and Engineering 2016; 138(12):121005.
[15] Moroni G, Petrò S, Polini W. Geometrical product specification and verification in additive manufacturing. CIRP Annals-Manufacturing Technology 2017; 66(1):157-160.
[16] Dantan JY, Huang Z, Goka E, et al. Geometrical variations management for additive manufactured product. CIRP Annals-Manufacturing Technology 2017; 66(1):161-164.
[17] Zhu Z, Keimasi S, Anwer N, Mathieu L, Lihong Q. Review of Shape Deviation Modeling for Additive Manufacturing. In: Advances on Mechanics, Design Engineering and Manufacturing. Springer International Publishing; 2017. p. 241-250.
[18] Zhu Z, Anwer N, Mathieu L. Deviation Modeling and Shape transformation in Design for Additive Manufacturing. Procedia CIRP 2017; 60:211-216.
[19] Anwer N, Ballu A, Mathieu L. The skin model, a comprehensive geometric model for engineering design. CIRP Annals-Manufacturing Technology 2013; 62(1):143-146.